Institut Polytechnique
de Paris

LABORATOIRE
MAP5

Internship Report

Zhanbo Huang

Internship Duration: 05.2025 – 08.2025

Supervisor: Prof. Assaf Shapira

A report submitted in partial fulfilment of the requirements of
Institut Polytechnique de Paris
Master of Science in *Applied Mathematics and Statistics*

August 22, 2025

Abstract

This report investigates the relaxation dynamics of kinetically constrained models (KCMs), with particular emphasis on the East, FA-1f, and Additive models. Combining mathematical analysis with large-scale Monte Carlo simulations, we examine how kinetic constraints influence both the transient and stationary behavior of interacting particle systems. The results show that exponential relaxation provides an accurate description of the long-time decay, with fitted parameters consistent with theoretical predictions. Logarithmic transformations reveal some trends that enable precise estimation of decay rates, and we find that the relaxation parameter λ depends approximately linearly on the facilitation probability p. Finally, the methodology developed here provides a foundation for extending the analysis to other kinetically constrained models, offering new insights into universality and model-specific features of constrained relaxation.

Keywords: kinetically constrained models, FA-1f model, relaxation dynamics, Monte Carlo simulation, statistical physics

Contents

Chapter 1

Introduction

1.1 Background

In this internship, I study Interacting Particle Systems (IPSs), focusing particularly on a class of physics models known as Kinetically Constrained Models (KCMs). These models are widely used to investigate the behavior of particles in systems exhibiting glassy dynamics.

KCMs are of significant interest in statistical physics because they capture essential features of glass-forming materials, where particle motion becomes highly restricted at low temperatures or high densities.

The following sections introduce the specific models analyzed, summarize relevant literature, and outline the guiding questions for this research.

1.2 Model Description

Kinetically Constrained Models (KCMs) are a class of continuous-time Markov processes in which the evolution depends only on the current configuration (the Markov property). Transitions occur at rates determined by the present state, and the waiting times between transitions are exponentially distributed.

To illustrate the main ideas, we begin with the unconstrained model. In this case, L particles are arranged on a one-dimensional lattice, and each particle can be in state 0 or 1. Transitions from 0 to 1 occur at rate p, while transitions from 1 to 0 occur at rate q, with $p + q = 1$.

However, the unconstrained model is often too simplistic for real physical systems, where particle movement is typically limited by local constraints. To better capture these dynamics, we introduce kinetic constraints, which restrict state changes based

on the configuration of neighboring sites. The models considered in this report are summarized below:

1. **Unconstrained model:** No kinetic constraints; each particle flips independently at rates p and q.
2. **FA-1f Model (Fredrickson-Andersen one-spin facilitated):** A particle can change its state only if at least one of its neighbors is in state 0.
3. **East Model:** A particle can change its state only if its right (east) neighbor is in state 0.
4. **Addictive model:** If both neighbors are in state 0, the transition rate is p or q; if only one neighbor is in state 0, the rate is halved ($p/2$ or $q/2$).

These models enable a systematic study of how different kinetic constraints influence the relaxation dynamics and collective behavior of interacting particle systems.

It is clear that the strength of the kinetic constraint increases in the order: East $>$ Additive $>$ FA-1f $>$ Unconstrained.

1.3 Literature Review

Most of the results and theoretical analysis will be based on the book Hartarsky and Toninelli (2024).

Theorem 1.3.1 (Exponential convergence in all dimensions (Hartarsky and Toninelli, 2024, Theorem 7.6))**.** *Consider the FA-1f model on $\mathbb{Z}^d$ with $q \in (0,1]$. Fix $x \in \mathbb{Z}^d$ and an initial configuration $\omega \in \Omega$ such that $\omega_{x+\mathbb{N}^d} \neq 1_{x+\mathbb{N}^d}$. Then there exists $m = m(\omega, q) > 0$ and for each local function f with support contained in Δ_x^d there exists $C = C(f, \omega, q)$ such that for $t > 0$ sufficiently large it holds that*

$$|\mathbb{E}_\omega(f(\eta(t))) - \mu(f)| \leq Ce^{-mt}.$$

As established in Theorem 7.6 (Exponential convergence in all dimensions) of Hartarsky and Toninelli (2024), the East model exhibits exponential convergence under suitable conditions.

However, these results are obtained in an idealized mathematical setting. A natural question arises: will similar exponential convergence be observed in more realistic or practical scenarios? Furthermore, does this behavior extend to other kinetically

constrained models? Addressing these questions is one of the main motivations of this report.

1.4 Proposed questions

The whole internship and report will be guided by the following questions:

1. What is the fitting function for the density decay of the East model? Is the decay exponential? If so, what type of exponential behavior is observed?

2. Do the East model and the Additive model also exhibit exponential convergence? If so, what parameters characterize this convergence?

3. What is the behavior of the ρ function when starting from an initial density of 1, with only one boundary site active (empty)? Does this behavior apply to all three models?

Chapter 2

Mathematical Results

This section presents analytical results for the unconstrained and kinetically constrained models, focusing on the evolution of particle density and stationary measures. These results form the theoretical basis for interpreting the simulation data in later chapters.

2.1 Unconstrained Model

In this section, we present results for the unconstrained model, which serves as a baseline for comparison with kinetically constrained models (KCMs). Readers can refer to 1.2 for the seetings of the model.We now present the evolution function of the model.

Theorem 2.1.1 (Density Evolution in the Unconstrained Model)**.** *Let $\rho(t)$ denote the probability that a particle is in state 1 at time t in the unconstrained model, with initial condition $\rho(0) = \rho_0$. Then $\rho(t)$ satisfies*

$$\rho(t) = p + (\rho_0 - p)e^{-t}, \tag{2.1}$$

where p is the transition rate from state 0 to state 1.

Proof. The evolution of $\rho(t)$ is governed by the Kolmogorov forward equation:

$$\frac{d}{dt}P_t f = P_t(Qf) = Q(P_t f).$$

For each particle in the system, the master equation is given by:

$$\frac{d}{dt}P_1(t) = p\,P_0(t) - q\,P_1(t),$$

where $P_0(t)$ and $P_1(t)$ denote the probabilities of being in states 0 and 1, respectively, and q is the rate for transitions from state 1 to state 0. Note that $P_0(t)+P_1(t)=1$.

In a large system, since all the particles are independent. we define $\rho(t)$ as the density of particles in state 1, so the equation becomes

$$\frac{d\rho}{dt} = p \cdot (1-\rho(t)) - q \cdot \rho(t),$$

with initial condition $\rho(0) = \rho_0$. This is a first-order linear ordinary differential equation. Its solution is

$$\rho(t) = p + (\rho_0 - p)e^{-t}.$$

□

Therefore, by analogy, we expect that the evolution function for models such as the East model or FA-1f model will also follow an exponential relaxation, though with different parameters reflecting their kinetic constraints.

2.2 Stationary Measure

In this section, we examine the stationary measure, representing the long-term density of occupied sites. All models considered here admit a unique stationary measure, as they are irreducible, recurrent, and nonexplosive (excluding absorbing states such as the fully occupied configuration).

For the unconstrained model, Theorem 2.1.1 shows that the stationary density approaches p as $t \to \infty$. The FA-1f model admits a similar result: its stationary measure also converges to p.

Proposition 2.2.1 (Stationary Measure for the FA-1f Model)**.** *Let Λ be a finite lattice, and consider the FA-1f model on Λ, where each site $x \in \Lambda$ can be either* 0 *or* 1*. Then the unique stationary (invariant) measure of the FA-1f model is the product Bernoulli measure ν_p on $\{0,1\}^\Lambda$ with parameter $p \in (0,1)$.*

Explicitly, for any configuration $\eta \in \{0,1\}^\Lambda$, the stationary measure is given by

$$\nu_p(\eta) = \prod_{x\in\Lambda} p^{\eta_x}(1-p)^{1-\eta_x},$$

where $\eta_x = 1$ if site x is occupied, and $\eta_x = 0$ if site x is empty.

Proof. For the proof of the proposition, we are going to use the fact the reversibilty implies stationarity.

Let $\eta \in \{0,1\}^{\Lambda}$ be a configuration, and let η^x denote the configuration obtained from η by flipping the state at site $x \in \Lambda$, i.e.,

$$\eta_y^x = \begin{cases} 1 - \eta_x & \text{if } y = x, \\ \eta_y & \text{if } y \neq x. \end{cases}$$

Suppose that the update at x is allowed (i.e., the facilitation condition is satisfied). The rate for the transition from η to η^x is $c(x,\eta)$, which incorporates both the facilitation constraint and the flip probability.

The product measure ν_p satisfies the detailed balance (reversibility) condition:

$$\nu_p(\eta)\, c(x,\eta) = \nu_p(\eta^x)\, c(x,\eta^x)$$

for every allowed transition. Indeed, by direct computation,

$$\frac{\nu_p(\eta^x)}{\nu_p(\eta)} = \begin{cases} \dfrac{p}{q}, & \text{if } \eta_x = 0 \text{ and } \eta_x^x = 1, \\ \dfrac{q}{p}, & \text{if } \eta_x = 1 \text{ and } \eta_x^x = 0, \end{cases}$$

and the corresponding flip rates in the FA-1f dynamics are defined to match these ratios.

□

Therefore, we expect that the FA-1f model, the East model, and the Additive model will eventually converge to the same stationary density p as the unconstrained model. However, due to the presence of kinetic constraints, their evolution speed toward equilibrium will be different.

2.3 Decaying Behavior

Consider the following scenario: we start with an initial density of 1, with only the leftmost site being active, meaning it can change its state. As time evolves, the active state propagates to the right with a velocity v, which may depend solely on the parameter p.

At any time t, all sites to the left of the current active boundary are expected to have density p, while sites to the right retain density 1. The active boundary site will be located approximately at a distance vt from the left edge.

Based on this reasoning, we propose that the density function evolves as

$$\rho(t) = \frac{vt}{L}\, q + \frac{L - vt}{L} \cdot 1 = 1 - \frac{qvt}{L},$$

where the slope is $-\frac{qv}{L}$, and the corresponding relaxation time is approximately $\frac{L}{v}$. The resulting behavior will be presented in detail in Chapter 4, section 4.4.

2.4 Mean-Field Relaxation Dynamics

Motivated by the exact solution for the unconstrained model, we consider a unified mean-field framework to describe the time evolution of the density $\rho(t)$ for kinetically constrained models. We introduce a parameter $\alpha \in \{0, 1, 2, 3\}$ that characterizes the strength or nature of the kinetic constraint.

The general mean-field equation can be written as:

$$\rho'(t) \approx [p(1 - \rho(t)) - (1 - p)\rho(t)] \cdot (1 - \rho(t))^{\alpha} \cdot C, \tag{2.2}$$

where C is a model-dependent constant and α controls the facilitation strength: higher α corresponds to stronger kinetic constraints and slower relaxation.

Case $\alpha = 0$: No Constraint (Unconstrained Model)

In the absence of kinetic constraints, the evolution is governed by a simple exponential relaxation:

$$\rho(t) = p + (\rho_0 - p)\, e^{-\lambda t}, \tag{2.3}$$

where p is the stationary density, ρ_0 is the initial density, and $\lambda = 1$ for the unconstrained model.

To estimate λ from simulation data, we use the logarithmic linearized form:

$$\ln |\rho(t) - p| = \ln |\rho_0 - p| - \lambda t. \tag{2.4}$$

Plotting $\ln |\rho(t) - p|$ versus t allows direct estimation of λ via linear regression.

Case $\alpha = 1$: East and Additive Models

In these models, the kinetic constraint depends on the state of a single neighboring site. The mean-field differential equation is:

$$\rho'(t) \approx [p(1-\rho(t)) - (1-p)\rho(t)] \cdot (1-\rho(t)) \cdot C, \tag{2.5}$$

where C is a constant and p is the flip probability. This expression applies to both the East and Additive models in the mean-field setting.

The corresponding explicit solution satisfies:

$$\ln \left| \frac{p-\rho(t)}{1-\rho(t)} \right| \approx C_1 t + C_2, \tag{2.6}$$

where C_1 and C_2 are integration constants.

Case $\alpha = 2$

This model introduces a two-site kinetic constraint, although not of the standard FA-1f type. The facilitation term here does not reduce to a simple polynomial form like in the other models. The mean-field differential equation is:

$$\rho'(t) \approx [p(1-\rho(t)) - (1-p)\rho(t)] \cdot (1-\rho(t))^2 \cdot C, \tag{2.7}$$

where $\alpha = 2$, but the exact form of the solution is not currently known. This case is left open for further analysis.

$$\ln \left| \frac{p-\rho(t)}{1-\rho(t)} \right| + \frac{1-p}{1-\rho(t)} \approx C_1 t + C_2 \tag{2.8}$$

FA-1f Model: $(1-\rho^2)$ Constraint

Although not directly defined by a specific α value, the FA-1f model introduces a constraint term of the form $(1-\rho(t)^2)$, which corresponds to facilitation by either neighbor.

The mean-field differential equation is:

$$\rho'(t) \approx [p(1-\rho(t)) - (1-p)\rho(t)] \cdot \left(1-\rho(t)^2\right) \cdot C, \tag{2.9}$$

$$\ln \left| \frac{(1+\rho(t))^{1-p}(1-\rho(t))^{1+p}}{(p-\rho(t))^2} \right| \approx C_1 t + C_2, \tag{2.10}$$

Case $\alpha = 3$: FA-1f in the Dense Regime ($p \to 1$)

In this regime, the FA-1f model exhibits strong kinetic constraints because a site can only flip if at least one of its neighbors is vacant. When p is large (equivalently, the vacancy density $q = 1 - p$ is small), the dynamics become highly cooperative, leading to very slow relaxation.

The explicit solution for the mean-field approximation satisfies:

$$\frac{2}{p} \ln \left| \frac{p-\rho(t)}{1-\rho(t)} \right| - \frac{1}{2(p-1)(1-\rho(t))^2} + \frac{1}{1-\rho(t)} \approx C_1 t + C_2, \tag{2.11}$$

where C_1 and C_2 are integration constants.

From a rigorous perspective, Hartarsky and Toninelli (2024) proved that, in one dimension ($d = 1$), there exists a constant $C > 0$ such that for sufficiently small $q = 1 - p$,

$$\frac{1}{C} \leq q^3 T_{\text{rel}} \leq C, \quad \frac{1}{C} \leq q^3 \mathbb{E}_{\mu_q}[\tau_0] \leq C, \quad \mathbb{P}_\mu(\tau_0 > t) \leq e^{-Cq^3 t}, \tag{2.12}$$

where T_{rel} is the relaxation time, and τ_0 is the first hitting time of the origin in the stationary dynamics.

These results indicate that the characteristic relaxation timescale of the FA-1f model scales as q^{-3} as $q \to 0$. This scaling is consistent with an *effective* mean-field exponent $\alpha = 3$ in the dense regime, reflecting the highly cooperative and facilitated dynamics of the system.

Chapter 3

Simulation

3.1 Algorithm

This section describes the simulation algorithm used for all models in this report. We present the procedure for the FA-1f model as a representative example; other models differ only in their specific update rules.

The pseudocode below summarizes the main simulation steps. For complete implementation details, please refer to the accompanying GitHub repository. The full implementation and additional scripts used in this work are available at: https://github.com/Jazzzing/Kinetically-Constrained-Model-Simulation.

Algorithm 1: FA-1f Kinetic Monte Carlo Simulation

for *each site* i **do**
    Compute flip rate at i based on neighboring states;
    Mark i as active if the constraint is satisfied;
end
while $t < t_{\text{max}}$ *and active sites exist and* $k < N_{\text{points}}$ **do**
    Compute total rate R;
    Draw $\Delta t \sim \text{Exp}(1/R)$ and update $t \leftarrow t + \Delta t$;
    Select site x to flip with probability proportional to its rate;
    Flip `config`$[x]$ and update affected neighbors;
    Compute current density $\rho(t)$;
    while $t \geq$ `fixed_times`$[k]$ *and* $k < N_{\text{points}}$ **do**
        Store $\rho(t)$ at index k;
        Increment k;
    end
end

3.2 Parameters setting

The simulation uses the following main parameters:

- **System size (`L`)**: Number of Particles (typically $L = 30,000$).
- **Flip rate (`q`)**: Probability that a site in state 1 flips to 0; $1p$ governs $0 \to 1$ flips.
- **Simulation time (`t_max`)**: Maximum time simulated, usually $t_{\text{max}} = 1,000$.
- **Initial density (`initial`)**: Fraction of sites initially in state 1 (e.g., p - 0.05).
- **Random seed (`seed`)**: For reproducibility, usually seed=42.
- **Number of runs (`num_runs`)**: Number of independent simulations for averaging (typically 200).
- **Temporal resolution (`N_points`)**: Number of time points where density is recorded, usually 500.

3.3 Tips for Codes

To reduce noise and improve the efficiency of our simulations, several strategies can be employed:

1. **Averaging Over Multiple Runs:**
   To obtain smoother curves and more reliable results, we run the simulation multiple times and compute the average across all runs, leveraging the law of large numbers. To further accelerate the overall process, we employ parallel execution by distributing the independent runs across multiple CPU cores. This strategy can significantly reduce the total runtime, potentially by a factor of two or more. We implement parallelism using Python's `concurrent.futures` library, which allows efficient management of multiple processes.

2. **Using Numba for Optimization:**
   Increasing the number of particles in the simulation improves the accuracy and reduces noise. However, this also increases the computational burden. To address this, we utilize `numba`, a just-in-time (JIT) compiler that can accelerate Python code by up to 40 times in this context. This is achieved through low-level optimization of array operations and tight computational loops, which are critical in large-scale stochastic simulations.

3. **Fixed-Time Recording Strategy:**
   Due to the stochastic nature of the model, different simulation runs can produce trajectories of varying lengths, which complicates the averaging process. To resolve this, we define a fixed set of time points and record the system's density only at those specific times. This approach standardizes the output format, simplifies post-processing, and reduces memory usage by avoiding unnecessary data storage.

4. **Cloud-Based Execution:**
   Running large-scale simulations on personal machines can be limited by hardware constraints and reliability issues such as unexpected shutdowns or network interruptions. To address this, we leverage cloud computing services, specifically Google Cloud Platform (GCP), to execute our simulations on virtual machines. This setup provides stable and scalable computational resources, allowing for uninterrupted long-duration tasks, better CPU performance, and easy integration with cloud storage services (e.g., Google Drive) for automated result backup and retrieval.

Chapter 4

Results

4.1 Time evolution

4.1.1 Initial Density $\rho_0 = 0$ (East Model)

Based on equation 2.3 in Section 2.4, we fit the simulation data using the exponential relaxation form

$$f(t) = A + Be^{-\lambda t^{\beta}}.$$

When $\beta = 1$, this reduces to a standard exponential fit, while values of $\beta < 1$ correspond to a stretched exponential fit. The fitting is carried out using Python's `curve_fit` function, and the results are presented in Figure 4.1. The simulation parameters are as follows:

$$L = 30,000,\ p = 0.8,\ \rho_0 = 0,\ t_{\text{max}} = 1,000,\ \text{seed} = 42,\ \text{num\_runs} = 200.$$

For the stretched exponential case, the fitted parameters satisfy $A \approx p$ and $B \approx \rho_0 - p$, in agreement with theoretical predictions. Although the regular exponential form captures the overall trend, it does not align well with our mathematical results, likely due to slower dynamics at early times. Since our primary interest lies in the asymptotic behavior, we focus on the long-time tail of the data. Additional results for simulations with higher initial density are presented in the next section.

4.1.2 Initial Density $\rho_0 = 0.75$ (East model)

The same fitting procedure is applied for $\rho_0 = 0.75$ with identical simulation parameters. Figure 4.6 displays the results.

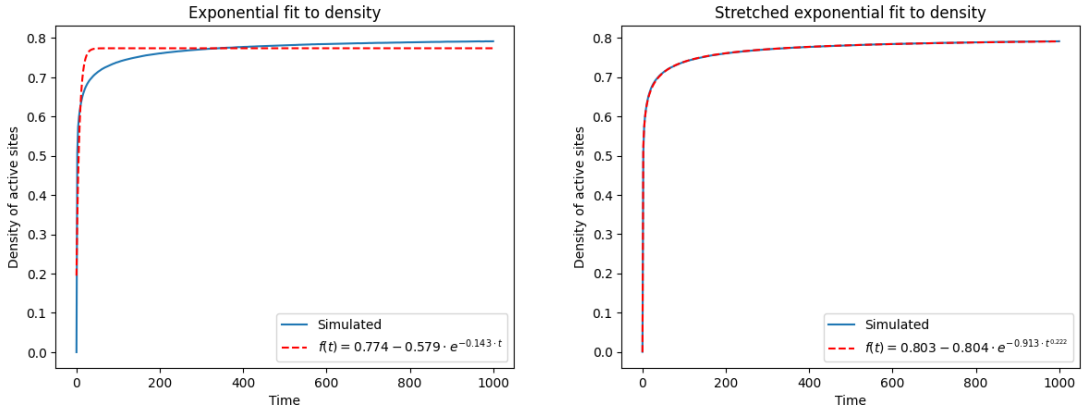

(a) Exponential fit (b) Stretched exponential fit

Figure 4.1: Comparison of exponential and stretched exponential fits for the FA-1f model ($\rho_0 = 0$).

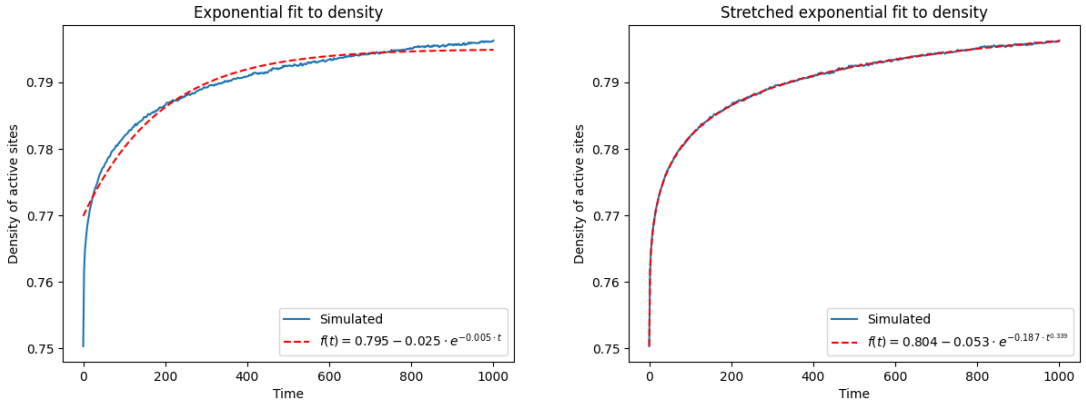

(a) Exponential fit (b) Stretched exponential fit

Figure 4.2: Exponential and stretched exponential fits for the East model with $\rho_0 = 0.75$.

For this case, the difference between the exponential and stretched exponential fits is minor, and both models describe the long-term decay with comparable accuracy. Therefore, we base our following analysis on the initial density that is closer to the final density ($\rho_0 = p - 0.05$). We acknowledge, however, that this assumption may not be entirely justified. This limitation will be discussed further in Chapter 5, and we encourage future researchers to refine and improve upon our approach.

4.2 Log-transformation

In this section, we examine the logarithmic transformation of the density function in order to explore its long-term behavior, in analogy with the analysis presented in

Section 2.4. In particular, we focus on the case where the initial density is chosen close to the final stationary density, as motivated in the previous section.

We use the following representative parameter set as an illustrative example (which is the same as the previous section):

$$L = 30,000, \quad p = 0.8, \quad \rho_0 = 0.75, \quad t_{\text{max}} = 1,000, \quad \text{seed} = 42, \quad \text{num\_runs} = 200.$$

Figure 4.3 compares log–transformed diagnostics for four choices of the facilitation exponent α; see Section 2.4 for the definition of α and the corresponding mean-field predictions.

For $\alpha \in \{0, 1, 2\}$ the transformed curves are essentially linear after $t = 200$, indicating an exponential approach of the diagnostic to its asymptote and agreeing with the mean-field analysis. The $\alpha = 3$ panel shows noticeable curvature over our finite time window, which is believed to be the limit of the t max.

Among the four diagnostics, the $\alpha = 1$ form,

$$\log|p - \rho(t)| = \log|1 - q - \rho(t)|\,,$$

is the most stable and interpretable in practice. The other panels can be viewed as simple (affine) transformations of this quantity, differing mainly by additive constants or terms that become negligible as $\rho(t) \to p$, and therefore do not convey additional information about the long-time slope.

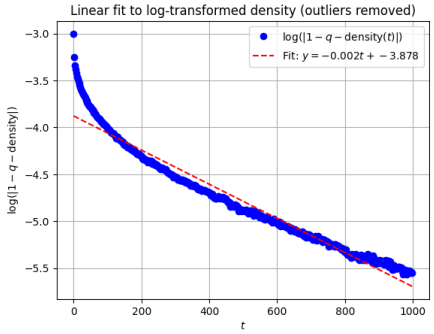

(a) Case: $\alpha = 0$

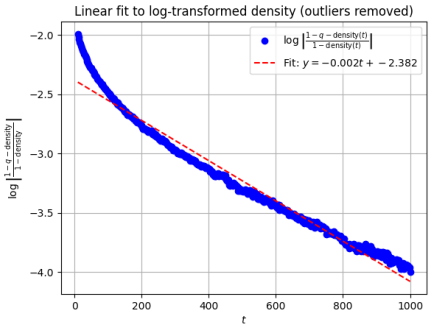

(b) Case: $\alpha = 1$

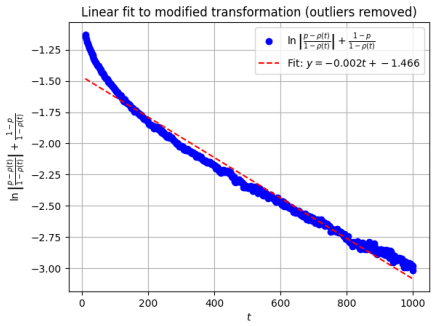

(c) Case: $\alpha = 2$

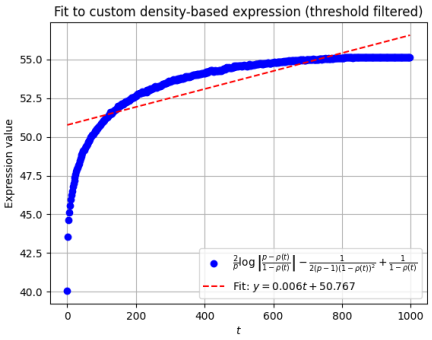

(d) Case: $\alpha = 3$

Figure 4.3: Log-transformed relaxation dynamics for different values of α with parameters $p = 0.8$, $\rho_0 = 0.75$.

4.3 Decay rate λ versus p

Building on the analysis of the previous section, where the logarithmic transformation yielded a linear relation suitable for quantitative study, we now examine the dependence of the decay rate λ on the parameter p. From Figure 4.3, we observe that the transformed curves become essentially linear for $t \gtrsim 300$. Consequently, we restrict our fits to this late-time regime. The simulation parameters are kept identical to those in the previous sections.

4.4 Decaying behavior

With initial density $\rho(0) = 1$ and a single active site at the left boundary, the active front propagates rightward with velocity v. Following the heuristic in Section 2.3,

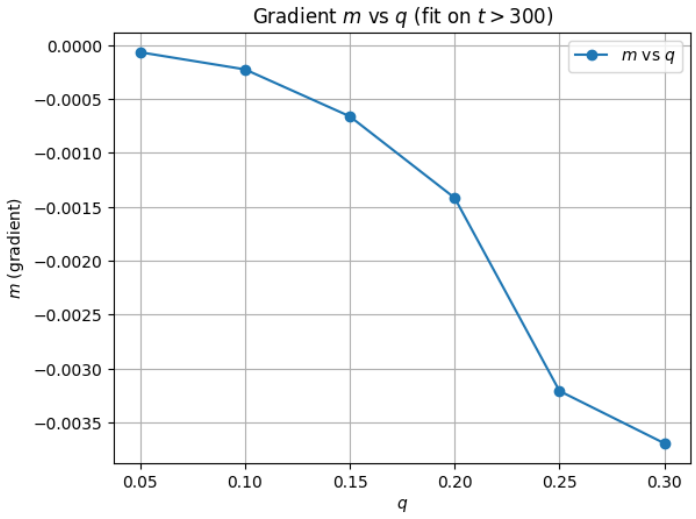

Figure 4.4: Decay rate λ as a function of p.

the spatially averaged density evolves as

$$\rho(t) = \frac{vt}{L}q + \frac{L - vt}{L} \cdot 1 \;=\; 1 - \frac{qv}{L}\,t,$$

So the slope is $m = -qv/L$ and the relaxation time (when the front reaches the right edge) is $t_\star \simeq L/v$.

Empirical laws Across all runs considered (FA-1f, East, and the additive model), the density exhibits a linear–decay regime followed by a plateau. The data are consistent with the following relations:

$$\rho(t) \simeq 1 - \frac{q\,v(p)}{L}\,t, \qquad 0 \le t \lesssim t_\star, \tag{4.1}$$

$$m(L,p) = -\frac{q\,v(p)}{L}, \tag{4.2}$$

$$t_\star(L,p) \simeq \frac{L}{v(p)}, \qquad \rho(\infty) = p. \tag{4.3}$$

Here m is the fitted slope of the linear–decay regime and $v(p)$ is the front velocity.

For example, for $(L,q) = (2000, 0.8)$, see the figure 4.5, we measure $m = -2.43 \times 10^{-4}$, giving

$$v = \frac{-mL}{q} \approx 0.61 \text{ sites/time}, \qquad t_\star^{\text{pred}} = \frac{L}{v} \approx 3.29 \times 10^3,$$

which matches the observed onset of the plateau and the fitted level $\rho(\infty) \approx 1-q = 0.2$.

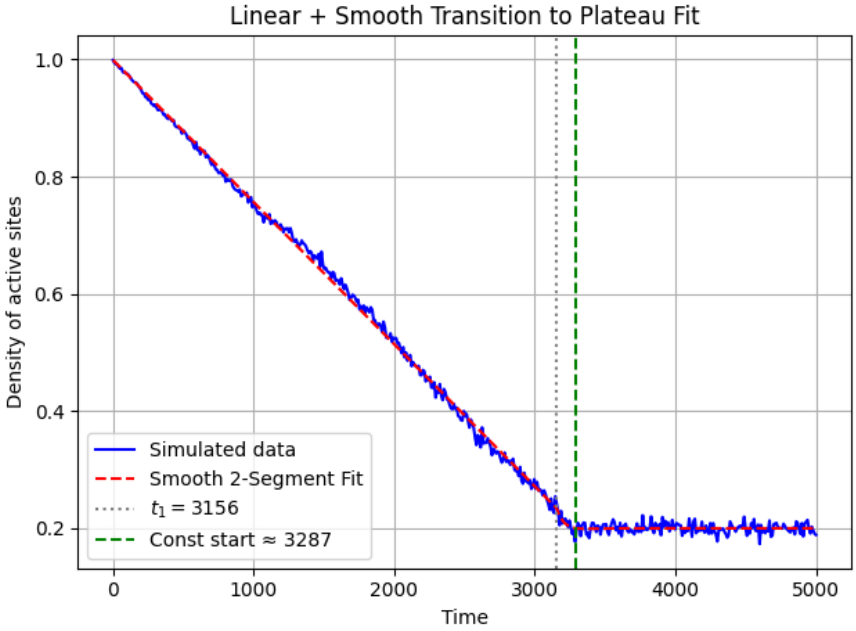

Figure 4.5: Density decay in the FA-1f model for $L = 2000$ and $q = 0.8$. The blue curve is the simulated data, the red dashed line is the smooth fit, and the vertical lines mark the transition to the plateau region.

Independence on system size. From the measurements of v at fixed $p = 0.1$ for several L (Fig. 4.6a), we find that

$$v(L; p = 0.1) \approx \text{constant}(0.79), \tag{4.4}$$

i.e. the front velocity is *independent of the system size* L within our numerical precision.

Dependence on facilitation probability. At fixed $L = 1000$ (Fig. 4.6b), the measured velocity decreases monotonically with p:

$$v = v(p), \qquad v'(p) < 0, \tag{4.5}$$

so larger p (equivalently smaller $q = 1 - p$) yields slower propagation and from the 4.6b, it has a linear dependency.

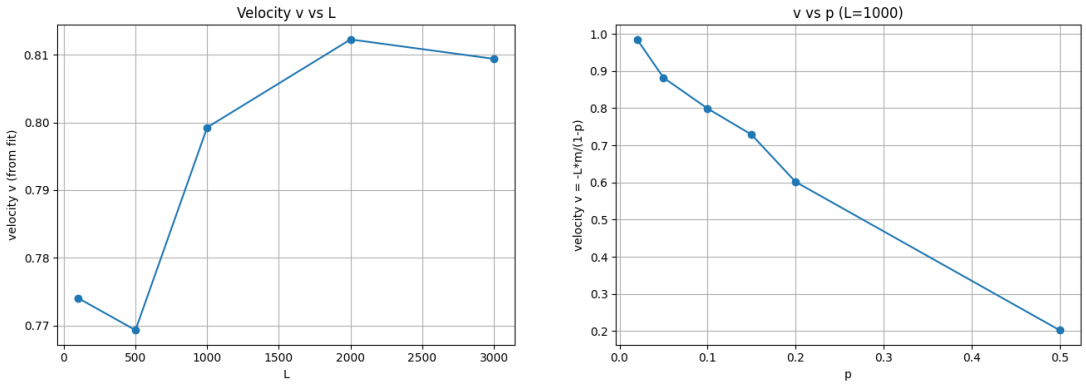

(a) Exponential fit

(b) Stretched exponential fit

Figure 4.6: Exponential and stretched exponential fits for the FA-1f model with $\rho_0 = 0.495$.

Model comparison. All three dynamics (FA-1f, East, additive) display the same linear–decay/plateau structure and satisfy (4.2)–(4.3); moreover, FA-1f and East give nearly indistinguishable $v(p)$, with the additive model closely similar.

Chapter 5

Prospective Work

5.1 Logarithmic Performance

As discussed in Section 4.1, the regular exponential form is generally sufficient for describing the relaxation dynamics. However, the role of the stretched exponential parameters, particularly β, remains somewhat unclear. A deeper theoretical analysis is needed to determine whether the stretched form provides genuine additional insight or whether the regular exponential description is adequate in all relevant regimes.

5.2 Exploring More Models

This report has primarily focused on the East model as a representative case. Nonetheless, the methodology developed here is directly applicable to other kinetically constrained models, such as the FA-1f and Additive models. Extending the analysis to these systems will allow for systematic comparisons across different types of kinetic constraints. Such comparisons are expected to provide valuable insights into commonalities and differences between models, and to shed light on the universality of exponential versus stretched relaxation behavior.

References

Hartarsky, I. and Toninelli, C. (2024), *Kinetically Constrained Models*. Manuscript, December 19, 2024.
URL: *https://doi.org/10.48550/arXiv.2412.13634*